BOHR Journal of Biocomputing and Nano Technology
2023, Vol. 1, No. 2, pp. 52–57
DOI: 10.54646/bjbnt.2023.11
www.bohrpub.com

METHODS

Method of anisotropic deformation of elastic materials based on free-form patches

Sergey I. Vyatkin* **and Boris S. Dolgovesov**

Synthesizing Visualization Systems Laboratory, Institute of Automation and Electrometry, Siberian Branch, Russian Academy of Sciences, Novosibirsk, Russian Federation

***Correspondence:**
Sergey I. Vyatkin,
sivser@mail.ru

Received: 10 August 2023; **Accepted:** 18 August 2023; **Published:** 24 August 2023

A method of anisotropic deformation of elastic materials based on free-form patches for biomechanics problems is presented. The method provides an analysis of the anisotropic hyperelasticity of transverse isotropy. For this purpose, fast and efficient Newton solutions are used. An invariant of anisotropic deformation is proposed, with the help of which side states of energy are eliminated at large deformation. The method is also used to restore finite elements. Because of this, it is possible to model large deformations, including for grids containing degenerate elements.

Keywords: perturbation functions, free-form patches, anisotropic deformation

Introduction

In problems of trajectory optimization for articulated bodies are solved (1, 2). Differentiable dynamic models of an articulated body are used (3, 4). Anisotropic materials are used in biomechanics, which include biological tissues, such as skin and muscles (5). When modeling muscles, tissues, and so on, anisotropic energies are used, as it is impossible to solve this with the help of isotropic energies based on Newton's methods and gradients (6, 7). In Hahn et al. (8), materials with symmetry properties relative to three mutually perpendicular planes are considered, but the use of anisotropic energies in Newton's solutions is a problem, as there are only approximate methods and brute-force methods for returning the Hessian to semi-positive certainty. Modeling of elastic dynamic objects is used in interactive surgical simulators. A spectral decomposition method is proposed in Chen et al. (9). This method is used to simulate virtual surgery (10). Algorithms for modeling soft tissue deformation in virtual surgery are presented. With the help of these algorithms, the properties of the tissue material, the visco-elasticity of tissues, and the anatomy of tissues are simplified. The principles and components of a surgical simulator are also described. The process of creating a surgery simulator for a specific patient from a set of medical images is shown. Based on the perturbation functions (11, 12), an approach was proposed (13), which includes the use of control of the musculoskeletal system. Dynamic destruction surrounds us in our daily life, but it is known that it is extremely difficult to revive this phenomenon and is even more complicated by anisotropic materials-materials with underlying structures that dictate the preferred directions of destruction. The paper (14) presents a method for the evolution of anisotropic damages, an algorithm for anisotropic elastic response, and an approach to conjugation. The geometric approach of mechanics is used for anisotropic damage. It is supplemented with structural tensors to encode the anisotropy of the material. In Mu et al. (15), a method of robotic cutting of soft materials is described, which can be used for surgical manipulations. Simulators make it easier to check controllers and generate data sets. Differentiable simulators provide radiation-based optimization. This is important for the calibration of simulation parameters and optimization of controllers. Smooth movements of the knife carry out the cutting of the material. The knife overcomes the impact strength of the material, counteracts the friction of the blade material, and creates a deformation of the shape. The paper describes the control of a robotic arm. As mentioned

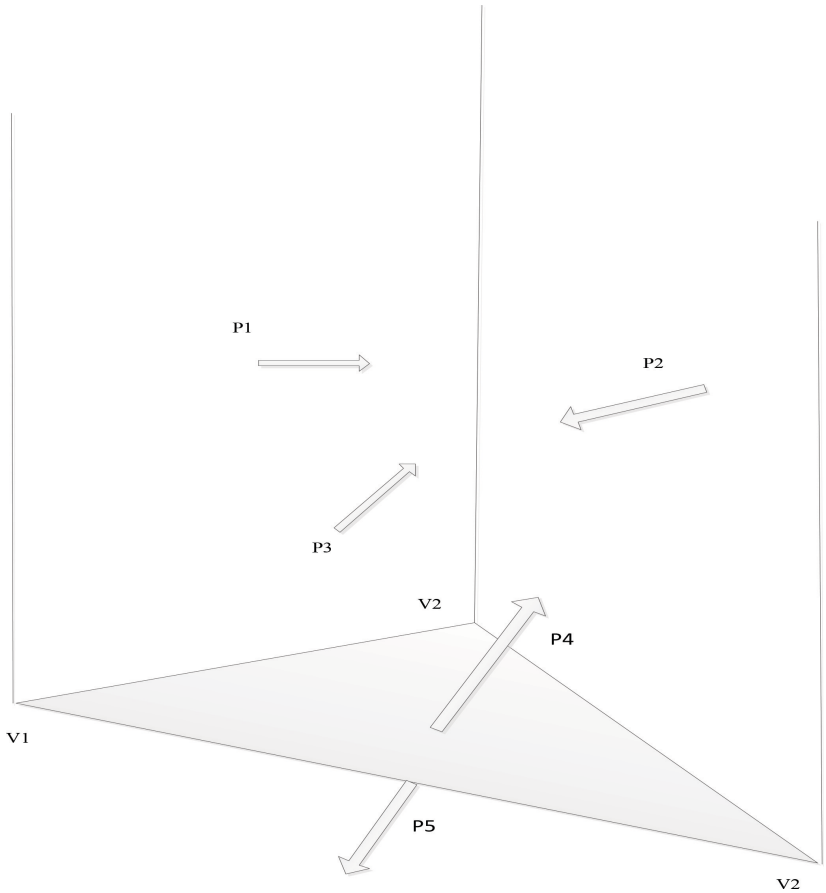

FIGURE 1 | Base triangle.

above, the application of anisotropic energies to Newton's solutions is a problem, as there are only approximate methods and brute-force methods.

In the proposed study, this problem is solved using anisotropic energy, which is used in biomechanics, and has its own closed-form compositions. Anisotropic energies having the same eigenvectors are used. The only change is manifested in the eigenvalues. The results are used in the implementation of fast and efficient Newton solutions. Existing transversely isotropic energies contain false stable states. This leads to non-physical states during modeling. To exclude this, an invariant of anisotropic deformation is proposed. A simple and reliable anisotropic energy is used. As the energy is quadratic, it is used for both the introduction of anisotropic hardening and softening to isotropic models. For its own system, expressions are presented in closed form. Anisotropic energies are also used to restore poorly conditioned elements. As a result, large deformations are reliably modeled and the number of conditions of the finite Hessian is reduced. In the proposed method, the proper systems of anisotropic energies are expressed in a closed form. The invariant of anisotropic deformation takes into account the inversion. An anisotropic model adapted for inversion is used. These solutions allow us to reliably and efficiently model poorly conditioned elements. In this paper, we study the transverse isotropy. This transverse case allows us to make a factorization of an isotropic material. It also does not depend on the choice of basic functions. The paper also considers the problem of retargeting at rest. When animating, the high-quality grid is distorted to match the input animation. During deformation, the quality of the grid decreases, but full correction (relaxation) in each frame is an expensive operation. The relaxation method is used to improve the quality of a curved mesh without changing its topology. To do this, as much of the model of the isotropic material as possible is preserved. This also eliminates a sharp increase in the number of conditions.

Method description

Free-form patch

A description of complex geometric models using free-form patches is proposed. Free-form patches are constructed by setting the perturbation functions from the base triangles (11; **Figures 1–3**).

Here, v1, v2, and v3 represent the base triangle; p1, p2, and p3 are the clipping planes; and p4 and p5 are the base planes (**Figure 1**).

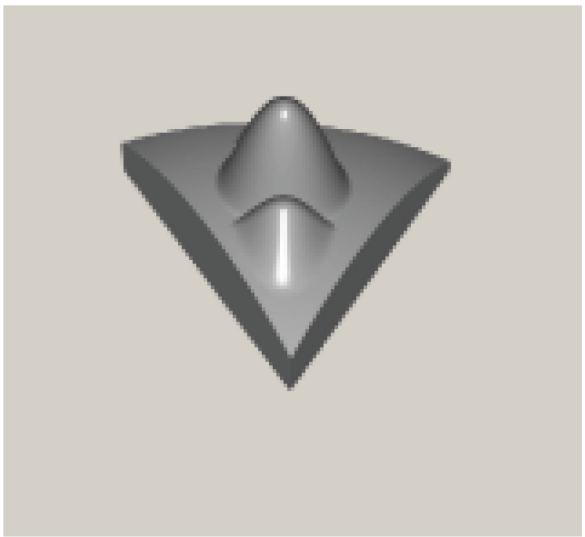

FIGURE 2 | Free-form patch.

A free-form patch is formed using perturbation functions relative to the base triangle: $F'(\vec{p}) = F(\vec{p}) + \sum_{i=1}^{N} R_i(\vec{p})$

$$R_i(\vec{p}) = \begin{cases} Q_i^3(\vec{p}), \ if \ Q_i(\vec{p}) \geq 0 \\ 0, \ if \ Q_i(\vec{p}) < 0 \end{cases}, \tag{1}$$

where $(\vec{p})$ is the 3D point, $R(\vec{p})$ is the perturbation function, and $Q(\vec{p})$ is the perturbing quadric.

Anisotropic deformation

The deformation map $map(\bar{x}) = \mathbf{x}$ is applied, and the vertex is deformed from the initial position$\bar{x}$ to the new position **x**. The following affine map is applied $map(\bar{x}) = S(\bar{x}) + t$. Here, $t \in \Re^3$ determines the translation, and $S \in \Re^{3x3}$ determines the scaling and rotation of the map, which is called the deformation gradient. Their union determines the shift, while $\partial map(\bar{x})/\partial \bar{x} = S$. The vertex offset is denoted as **s;** $\mathbf{x} = \bar{x}$ + **s** is the new coordinate.

The forces are calculated using the basis change tensor and double compression (16):

$$c = \partial S^T/\partial s \ : \frac{\partial \Xi(S)}{\partial S}, \tag{2}$$

where $\Xi(S)$ is the deformation energy.

For patches of free forms, $c \in \Re^{12}$, $\frac{\partial \Xi(S)}{\partial S} \in \Re^{3x3}$, and $\partial S^T/\partial s \in \Re^{3x3x12}$.

We write down the isotropic deformation energy (17)

$$I_{S^TS} = tr(S^TS), II_{S^TS} = tr((S^TS)^T, S^TS), III_{S^TS} = \det(S^TS), \tag{3}$$

In addition, we define the anisotropic invariants (18)

$$IV_{S^TS} = a^T(S^TS)a, V_{S^TS} = a^T(S^TS)^T(S^TS)a, \tag{4}$$

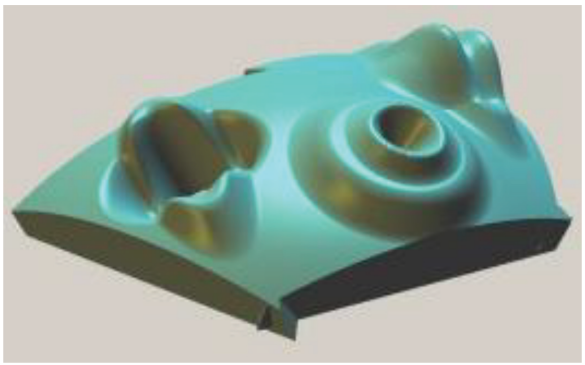

FIGURE 3 | Three free-form patches.

where a is the direction of anisotropy.

Let the Hessian in three-dimensional space be expressed in the form (19)

$$\frac{\partial tr((S^TS)(aa^T))}{\partial S} = 2S(aa^T), \tag{5}$$

$$\frac{\partial^2 tr((S^TS)(aa^T))}{\partial s} = 2\begin{bmatrix} (aa^T)_{00}I_{3x3} & (aa^T)_{01}I_{3x3} & (aa^T)_{02}I_{3x3} \\ (aa^T)_{10}I_{3x3} & (aa^T)_{11}I_{3x3} & (aa^T)_{11}I_{3x3} \\ (aa^T)_{20}I_{3x3} & (aa^T)_{21}I_{3x3} & (aa^T)_{22}I_{3x3} \end{bmatrix}, \tag{6}$$

where I_{3x3} is a 3 × 3 identification matrix and $(aa^T)_{ij}$ is a scalar entry (i, j) (aa^T).

The Hessian of arbitrary energy Ξ_5 (19) is

$$\frac{\partial^2 \Xi_5}{\partial s^2} = \frac{\partial \Xi_5}{\partial I_5}\frac{\partial^2 I_5}{\partial s^2} + \frac{\partial^2 \Xi_5}{\partial I_5^2}\left(\frac{\partial I_5}{\partial s}\frac{\partial I_5^T}{\partial s}\right), \tag{7}$$

Substituting (4) and (5) into this expression gives

$$\frac{\partial^2 \Xi_5}{\partial s^2} = 2\left[\frac{\partial \Xi_5}{\partial I_5}\begin{bmatrix} (aa^T)_{00}I_{3x3} & (aa^T)_{01}I_{3x3} & (aa^T)_{02}I_{3x3} \\ (aa^T)_{10}I_{3x3} & (aa^T)_{11}I_{3x3} & (aa^T)_{11}I_{3x3} \\ (aa^T)_{20}I_{3x3} & (aa^T)_{21}I_{3x3} & (aa^T)_{22}I_{3x3} \end{bmatrix} + 2\frac{\partial^2 \Xi_5}{\partial s^2}\left(vec(Saa^T\right)(vec(S(aa^T)^T)\right], \tag{8}$$

The vector $vec(Saa^T)$ is defined in the interval of a subspace of the third rank.

Let the twisting matrix be expressed in the form (20):

$$M_1 = UT_xAV^Taa^T, \tag{9}$$

Let the twisting matrix with rotations be expressed in the form (20):

$$M_2 = (\delta_y(V^Ta))UT_zAV^Taa^T - (\delta_z(V^Ta))UT_yAV^Taa^T, \tag{10}$$

where δ_y and δ_z are the diagonal elements of the matrix.

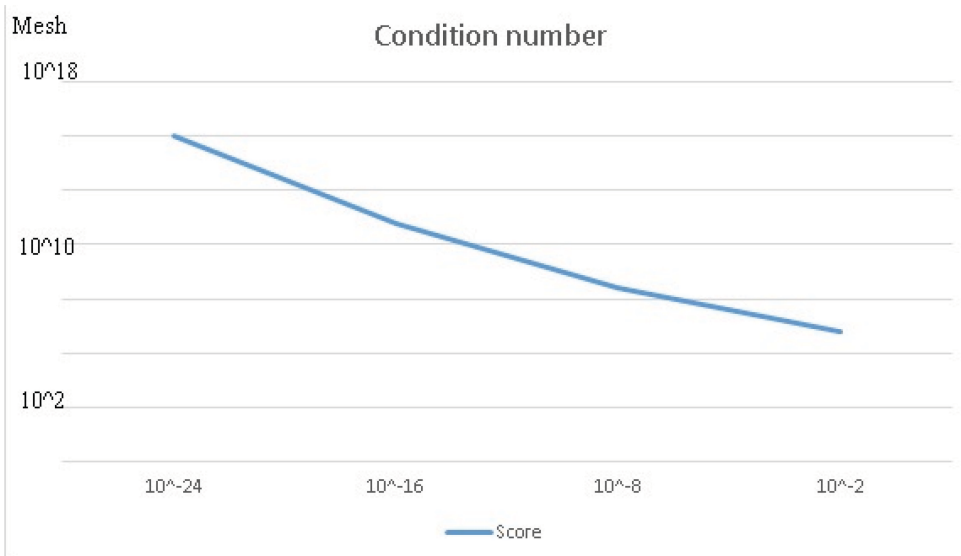

FIGURE 4 | Graph of the dependence of the score on the mesh.

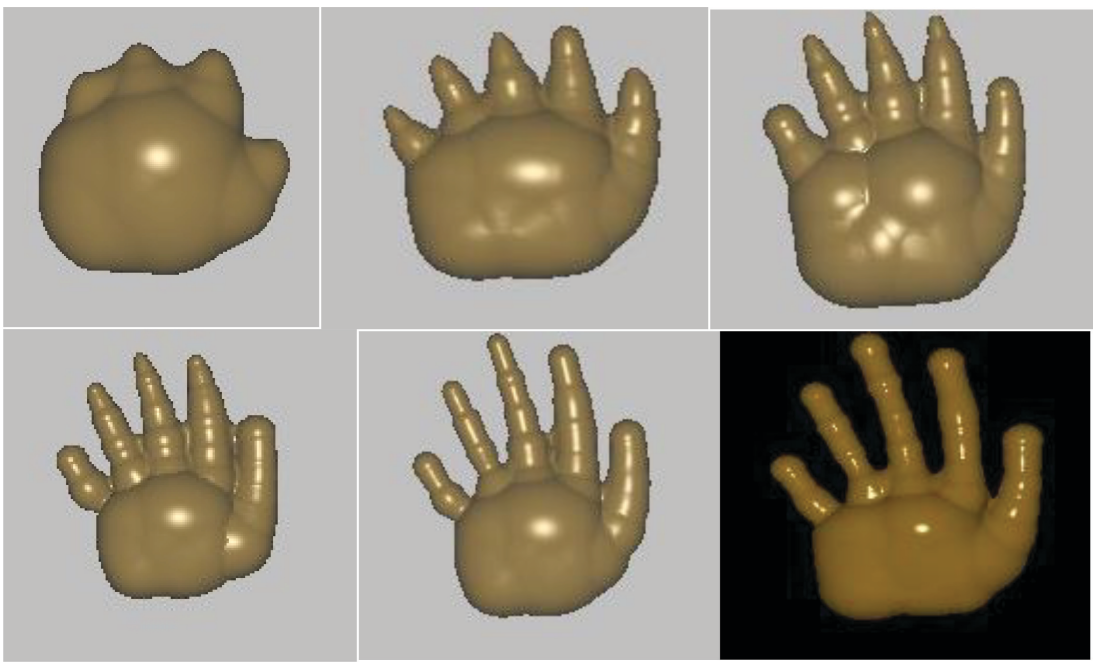

FIGURE 5 | The restored elements allow you to complete the sequence.

We use the substitution $(S^TS)_{\rightarrow}(R^TS)$:

$$I_a = tr((R^TS)aa^T), \tag{11}$$

Using a rotation gradient in a closed form using its own matrix:

$$M_e = \frac{1}{\sqrt{2}} U \begin{bmatrix} 0 & -1 \\ 1 & 0 \end{bmatrix} V^T, \tag{12}$$

Applying double compression, we get

$$\frac{\partial R}{\partial S} : Saa^T = \sqrt{2}(V^Ta)_x(V^Ta)_y \left(\frac{\delta_x - \delta_y}{\delta_x + \delta_y}\right) M_e, \tag{13}$$

Thus, an anisotropic invariant was used, and anisotropic energy was applied on its basis. The positive property of this invariant is that the stretching in the direction of the fiber is controlled.

Results

New strain gradients are proposed; therefore, new basis change tensors are applied. These tensors depend only on the positions in the space of objects, so the anisotropic case is simple. A simulation using these tensors is carried out, and

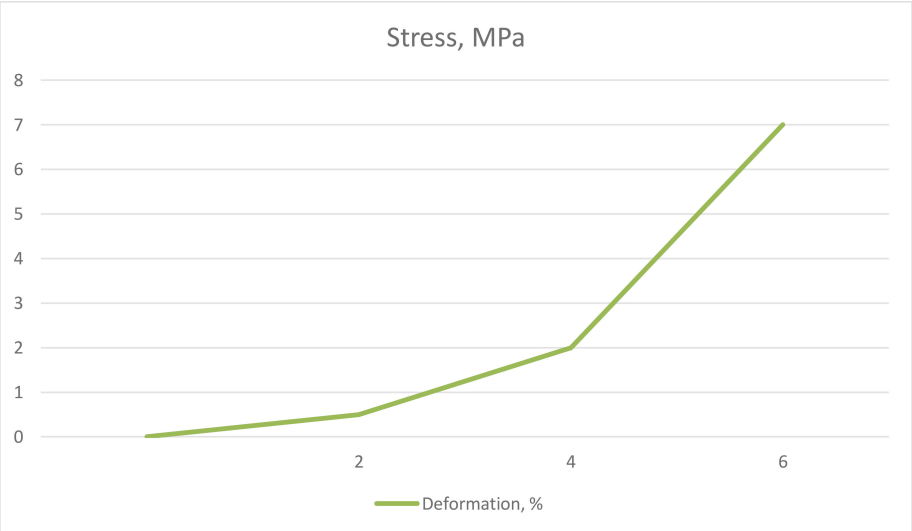

FIGURE 6 | Stress-deformation graph.

it is shown that the differences are visually insignificant. All components of element recovery are correct. 3D stretching tests were carried out on a grid containing 1,00,000 free-form patches with materials uniformly set for $\mu^{\circ}=^{\circ}1$ and $\lambda^{\circ}=^{\circ}100$ (**Figure 4**).

Based on these experiments, if it is assumed that the global conditionality will collapse by more than two orders of magnitude, rehabilitation is applied. In all the three-dimensional isotropic energies considered by us, this corresponds to $k \approx 10^{-5}$. The anisotropic model was calculated in 1.2 s per frame at $\mu^{\circ}=^{\circ}10$ when running on Intel Core i5-760 (four cores and four threads). In the case of softening, the mesh becomes very elastic; the model allows you to reliably process the dynamics. The simulation uses relaxation, but it diverges at the beginning of the sequence (**Figure 5**). The proposed method of rehabilitation allows you to complete the simulation. **Figure 6** shows the biomechanical behavior of the material (**Figure 5**) when it is loaded along the longitudinal axis in the form of a stress-deformation graph reflecting the dependence of deformation and stress. Stress is displayed on the ordinate axis, and deformation is displayed on the abscissa axis. When the material is stretched on the stress-deformation graph, a period of slight deformation (segment 0−2 on the abscissa axis) is revealed, which primarily depends on a thin elastin grid. The contribution of non-straightened collagen fibers to this phase can be neglected. In this phase, small loads cause strong stretching at low stress in the material. At the interval 2−4 of this graph, randomly located collagen fibers begin to arrange themselves in the direction of the force and straighten out. Deformation becomes more difficult. Later, on the segment 4−6, all collagen fibers are oriented in accordance with the direction of the force, and only slight deformation is possible.

Conclusion

The anisotropic energy optimal for inversion is presented. This energy is plain and reliable, which is developed using a proposed invariant. A method for restoring elements for poorly conditioned grids is proposed. This method is based on free-form patches. The method is capable of processing quadrature degeneracy for any grid. From the point of view of biomechanics, the basic physical properties of an elastic material, such as stress, extensibility, viscoelasticity, and anisotropy, are considered. A grid of elastin fibers is responsible for the stress. Extensibility is a response to mechanical action. It allows the material to stretch. Viscoelasticity includes creeping and stress relaxation. Creeping is observed when the force applied to the long-term stretching of the material causes its gradual elongation. The effects of viscosity are observed only when a force greater than the material usually meets *in vivo* is applied for a long period. With anisotropy, the grid of collagen fibers determines the preferred extensibility in a certain direction. Collagen and elastin fibers are more stretchable along this direction. The mechanical properties of an elastic material are determined not by fibers of a separate type, but by their mutual arrangement and influence on each other, i.e., the architectonics of connective tissue fibers. These properties are dynamic and change as the connective tissue fibers are rearranged under the influence of external and internal forces. The properties of contractility and extensibility of the material, although due to the same structures, depend on different characteristics of connective tissue fibers and do not have a direct relationship. There is some tendency to the inverse dependence of these properties taken together. However, in a single case, knowing one property, it is impossible to predict the second.

References

1. Pan Z, Ren B, Manocha D. GPU-based contact-aware trajectory optimization using a smooth force model. *Proceedings of the 18th annual ACM SIGGRAPH/Eurographics Symposium on Computer Animation, Los Angeles, July 2019*. (Vol. 1), Los Angeles, CA: (2019). p. 1–12. doi: 10.1145/3309486.3340246
2. Neuman SM, Plancher B, Bourgeat T, Tambe T, Devadas S, Reddi V, et al. Robomorphic computing: A design methodology for domain-specific accelerators parameterized by robot morphology. *Proceedings of the 26th ACM International Conference on Architectural Support for Programming Languages and Operating Systems, virtual-April 2021*. New York, NY: Association for Computing Machinery (2021). p. 674–86. doi: 10.1145/3445814.3446746
3. Plancher B, Neuman SM, Bourgeat T, Kuindersma S, Devadas S, Reddi V, et al. Accelerating robot dynamics gradients on a CPU, GPU, and FPGA. *IEEE Robot Automat Lett.* (2021) 6:2335–42. doi: 10.1109/LRA.2021.3057845
4. Murray S, Floyd-Jones W, Konidaris G, Sorin DJ. A programmable architecture for robot motion planning acceleration. *Proceedings of the 2019 IEEE 30th International Conference on Application-specific Systems, Architectures and Processors (ASAP), New York, USA, July 2019*. New York, NY: (2019). p. 185–8. doi: 10.1109/ASAP.2019.000-4
5. Jiang Y, Van Wouwe T, De Groote F, Liu C. Synthesis of biologically realistic human motion using joint torque actuation. *ACM Trans Graphics.* (2019) 38:1–12. doi: 10.1145/3306346.3322966
6. Nakada M, Zhou T, Chen H, Weiss T, Terzopoulos D. Deep learning of biomimetic sensorimotor control for biomechanical human animation. *ACM Trans Graphics.* (2018) 37:1–15. doi: 10.1145/3197517.3201305
7. Won J, Park J, Lee J. Aerobatics control of flying creatures via self-regulated learning. *ACM Trans Graphics.* (2018) 37:1–10. doi: 10.1145/3272127.3275023
8. Hahn D, Banzet P, Bern JM, Coros S. Real2Sim: Visco-elastic parameter estimation from dynamic motion. *ACM Trans Graphics.* (2019) 38:1-13. doi: 10.1145/3355089.3356548
9. Chen YJ, Levin DI, Kaufmann D, et al. EigenFit for consistent elastodynamic simulation across mesh resolution. *Proceedings of the SCA '19:The ACM SIGGRAPH / Eurographics Symposium on Computer Animation (SCA '19), July 26–28, 2019, Los Angeles, US, July 2019*. New York, NY: ACM (2019). p. 1–13.
10. Delingette H, Ayache N. Soft tissue modeling for surgery simulation. In: Ciarlet P editor. *Handbook of numerical analysis*. Rocquencourt: Inria (2004). doi: 10.1016/S1570-8659(03)12005-4
11. Vyatkin S, Romanyuk A, Romanyuk O, Nechyporuk M, Chekhmestruk R, Mykhaylov P, et al. Optimized finite element method using free-form volume patches for deformation of three-dimensional objects. *Proceedings of the 10th International Conference on Advanced Computer Information Technologies (ACIT), Deggendorf, Germany, September 2020*. Deggendorf: (2020). p. 845–50. doi: 10.1109/ACIT49673.2020.9208817
12. Vyatkin S, Snigur A, Romanyuk A, Mykhaylov P, Nechyporuk M, Chekhmestruk R, et al. Deformation methods of functionally defined objects using perturbation functions. *Proceedings of the 10th International Conference on Advanced Computer Information Technologies (ACIT), Deggendorf, Germany, September 2020*. Deggendorf: (2020). p. 858–62. doi: 10.1109/ACIT49673.2020.9208808
13. Vyatkin S, Romanyuk O. Modeling and simulation of prosthetic gait using a 3D model based on perturbation functions. *BioArt Book: Teaching and Subjects on Bio-Medical Engineering*. Leuven: Leuven (Belgium) press (2021). p. 477–506.
14. Wolper J, Chen Y, Li M, Fang Y, Qu Z, Lu J, et al. AnisoMPM: Animating anisotropic damage mechanics. *ACM Trans Graphics.* (2020) 39:1-16. doi: 10.1145/3386569.3392428
15. Mu X, Xue Y, Jia YB. Robotic cutting: Mechanics and control of knife motion. *Proceedings of the 2019 International Conference on Robotics and Automation (ICRA), Montreal, Canada, May 2019*. Montreal, QC: (2019). p. 3066–72. doi: 10.1109/ICRA.2019.8793880
16. Golub H, Van Loan CF. *Matrix computations*. Baltimore, MD: JHU Press (2013). doi: 10.56021/9781421407944
17. Harris ME. A note on the green invariants in finite group modular representative theory. *Results Math.* (2008) 51:249–59. doi: 10.1007/s00025-007-0274-0
18. Liu IS. On representation of anisotropic invariants. *Int J Eng Sci.* (1982) 20:1099–109. doi: 10.1016/0020-7225(82)90092-1
19. Mohammad H, Santos SA. A structured diagonal Hessian approximation method with evaluation complexity analysis for nonlinear least squares. *Comput Appl Math.* (2018) 37:6619–53. doi: 10.1007/s40314-018-0696-1
20. Zhang JJ. Twisted graded algebras and equivalences of graded categories. *Proc London Math Soc.* (1996) 72:281–311.